SOFT ROBOTICS
Volume 6, Number 3, 2019

DOI: 10.1089/soro.2018.0059

SoRo
Soft Robotics

ORIGINAL ARTICLE

A Soft End Effector Inspired by Cephalopod Suckers and Augmented by a Dielectric Elastomer Actuator

Nick Sholl,[1,2] Austin Moss,[1,2] William M. Kier,[3] and Kamran Mohseni[1,2,4]

Abstract

This article describes a soft suction cup end effector with squid-inspired suction generation and an octopus-inspired cup design that uses a dielectric elastomer actuator (DEA) to generate suction for adhesion. The fabrication process for the end effector is described in detail, and a mechanical model for generated pressure differential as a function of voltage is presented. When actuated, the DEA exerts an electrostatic stress on the walls of the end effector, resulting in pressure reduction in its water-filled cavity. The actuator is soft, flexible, and creates suction without a reliance on typical DEA elements such as rigid supporting structures and elastomer prestrain. It does not require net fluid flux out of the sucker, allowing faster attachment and easier release. It can be actuated underwater and has been validated with pull-off tests. The sucker generates a pressure differential of 3.63 ± 0.07 kPa (±SD) when driven at 10.75 kV in water and should reach a 4.90 kPa pressure differential when energized at its theoretical failure point of 12.4 kV. Data normalized by the input voltage show that 90% of the maximum pressure differential can be achieved within 50 ms of voltage application. Weighing less than 30 g in air, this elastomer end effector is capable of pulling with a force of 8.34 ± 0.10 N (±SD) and reversibly lifting 26.7 times its own mass underwater when actuated at 10.75 kV.

Keywords: cephalopod, bioinspired, dielectric elastomer actuator, suction, grasping

Introduction

Cephalopod mollusks, such as octopuses, squids, and cuttlefish, have intrigued humanity for centuries. Despite their soft bodies, they are accomplished predators, using their muscular arms and tentacles for locomotion,[1] steering, prey capture,[2–5] and object manipulation, including the use of tools.[6] Attachment to and manipulation of prey or other objects by the arms and tentacles depend on powerful, muscular suckers.[7] Although there is considerable variation in the morphology of suckers among cephalopods, they generate adhesion by actively reducing the internal pressure relative to ambient pressure; in extreme cases, the pressure differential created is large enough to cause cavitation of the water in the cavity of the sucker.[8]

The soft robotic community has recognized the potential for using cephalopod-inspired suckers on robotic systems.[9–13] Such suckers could prove to be gentle, yet effective, mechanisms for attaching small autonomous underwater vehicles (AUVs), such as our group's CephaloBot[14] and daughter vehicle,[15] to a range of surfaces that vary in texture and compliance. Due to the high bulk modulus of water, once an effective seal with the surface is formed, only slight dilation of the enclosed volume is required to create relatively large suction forces in water. Lower actuation strains lead to lower power requirements, making an underwater bioinspired sucker an attractive choice for use on a compact AUV. Implementing a soft actuator such as this on a compact AUV, however, is nontrivial.

Innovation in the field of soft robotics has been hindered by the capability, availability, and manufacturability of soft actuators. Pneumatic and tension cable actuators have been widely used,[16,17] but they require rigid, often large support devices, such as motors, air compressors, or compressed air bottles, which are not easily supported by an AUV's resources. Shape memory alloy actuators have also been

[1]Department of Mechanical and Aerospace Engineering, University of Florida, Gainesville, Florida.
[2]Institute for Networked Autonomous Systems, University of Florida, Gainesville, Florida.
[3]Department of Biology, University of North Carolina, Chapel Hill, North Carolina.
[4]Department of Electrical and Computer Engineering, University of Florida, Gainesville, Florida.

explored,[10,18,19] but their actuation requires heaters with relatively high current draw, which reduces AUV battery life, especially when long-term actuation is needed. Dielectric elastomer actuators (DEAs), on the contrary, have shown the potential to reduce the need for heavy, bulky external support equipment while maintaining a large power density, low-power consumption, and fast actuation.[20,21]

Cephalopods use strong suckers on their arms and tentacles for prey capture, object manipulation, and locomotion. The suckers of octopuses are composed of a complex, three-dimensional (3D) array of muscle fibers, termed a ''muscular hydrostat,'' providing precise, active control of the deformation and stiffness of the sucker. Octopuses use the musculature of the suckers to actively induce stress in the water, creating a pressure differential for adhesion.[7,8,22] While the octopus uses other, more complex techniques and structures to maximize its suction potential while minimizing actuation effort,[23] the driving force behind octopus suction generation is active deformation of the sucker.

Squids and cuttlefish (decapod cephalopods) have suckers with more cylindrical internal cavities that are attached to the arms and tentacles by muscular stalks reinforced with connective tissues (Fig. 1). In addition to using the complex musculature of the suckers to create a pressure differential, the adhesion is likely augmented by pulling on the stalk once a seal with the substrate has been established. The cylindrical wall is reinforced with a layer of stiff material, most likely the protein chitin, and tension on the stalk pulls on the roof of the sucker, which functions in a manner similar to a piston in a cylinder. These stresses lower the pressure of the water in the cavity.[24] Decapod suckers have been suggested to be better candidates for a bioinspired device on a small, soft robot than octopus suckers due to their more passive and simple design.[24] They have also been shown to generate higher pressure differentials than octopus suckers.[25]

To our knowledge, there has been only one other successful attempt to use DEAs for suction generation.[27] The design presented in that work relies on a fluid-filled (pressurized), ellipsoidal bubble actuation unit with a stacked DEA on the top half of the bubble. When hydrostatically coupled with fluid in a suction cavity, the DEA creates a pressure differential within the cavity. As expected, increasing the volume of fluid within the bubble, and therefore the prestrain within the DEA layers, increases the pressure differential created by the actuator. While the researchers were successful in designing a DEA-driven device to create suction, their actuation module requires a rigid support frame to maintain a prestrain in the DEA layers and a pressure within the actuation module's bubble. These factors limit the versatility of the device for implementation into a fully soft robot. The pressurized bubble and hard frame could break under the large deformations expected of soft robotic systems, and the authors did not report test results of the device when submerged.

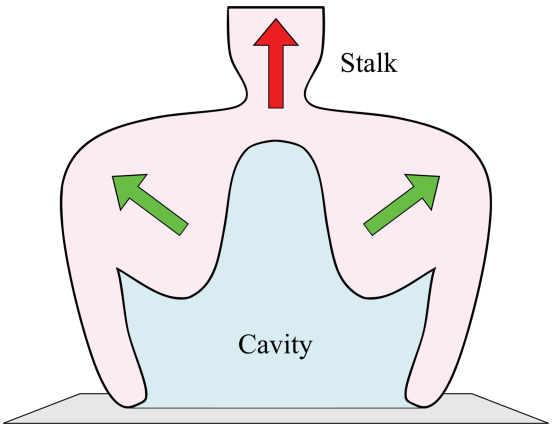

FIG. 1. Simplified longitudinal section of a squid sucker based on a study by Williams.[26] Squids create a pressure differential partially by contracting muscles in the direction of the *green arrows*. A muscular stalk connects the squid's suckers to its arms. Pulling on that stalk in the direction of the *red arrow* increases the generated pressure differential. Color images are available online.

In this article, we show that DEAs can be incorporated into a decapod-inspired suction device to help create a pressure differential that can be used to generate adhesive forces for many practical applications. By using DEAs to add an active element to the walls of a decapod-like sucker, we have created a bioinspired actuator that can create a seal on a substrate before any load is applied, without the need for net fluid flux out of the sucker. Since the actuator is designed to behave like a decapod sucker, which augments the pressure differential by pulling on the top of a cylindrical cavity with a tension-resisting stalk, loading the actuator significantly increases the pressure differential and suction force created. Moreover, since the sucker maintains a constant volume of fluid within its cavity, release does not require as much effort as traditional passive suction cups, which require peeling motions or excessive force to detach.

This article describes the design and fabrication process of the artificial sucker in detail in the Fabrication section before providing an overview of the models governing DEAs, mechanical interactions between the layers of the artificial sucker, cylindrical pressure vessels, and the transient behavior of the sucker in the Modeling section. We describe our procedure for evaluating the effectiveness of the design in the Experimental Procedure section and report our experimental results in the Results section. After discussing the behavior of the artificial sucker in the Discussion section, we summarize our conclusions and proposed future work in the Conclusions section.

Fabrication

The most important factor in decapod sucker suction generation is the tension stalk's effect on the sucker's wall stresses.[24] Forces applied to the stalk create significant pressure differentials, but DEAs alone have not yet shown the ability to create forces of a sufficient magnitude to generate those same pressure differentials. A useful actuator could, however, use DEAs in the walls of the sucker for creating a preliminary seal on a substrate before applying larger forces to the stalk to create the majority of the desired suction force. These larger forces need not be actively generated; they could be passively applied, such as by adhering to the bottom of the hull of a ship and using negative buoyancy of the AUV to pull on the stalks of the artificial suckers. Our artificial suckers are designed with the ability to actively or passively actuate the tension stalk to amplify the actuation of the DEA. We

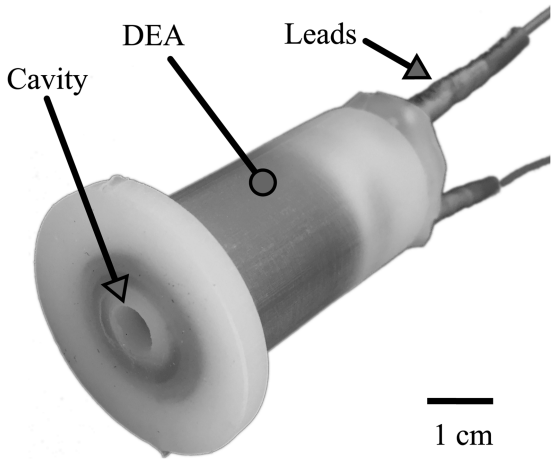

FIG. 2. Artificial sucker with Dragon Skin 10 inner core, VHB 4905 and carbon grease rolled DEA, Dragon Skin 10 skin, and electrode leads for fully soft sucker pressure generation tests. DEA, dielectric elastomer actuator; VHB, very high bond.

demonstrate the DEA's ability to generate a pressure differential in a fully soft configuration, and we also demonstrate the forces obtainable by this design by implementing a configuration with a 3D-printed attachment point as well.

To use this sucker on a robotic system, it must be attached to the main body of the robot. There are many ways of accomplishing this for both soft and rigid robots. For example, the sucker could be molded directly into a soft body, and thus no rigid components would be required. In this study, we chose to mold a 3D-printed, threaded attachment point into some of our suckers for pull-off and lifting tests (described in the Experimental Procedure section).

Our artificial suckers (Figs. 2 and 3) are composed of an elastomer inner core/suction cavity, a rolled DEA wrapped around the inner core (Fig. 4), a 3D-printed attachment point

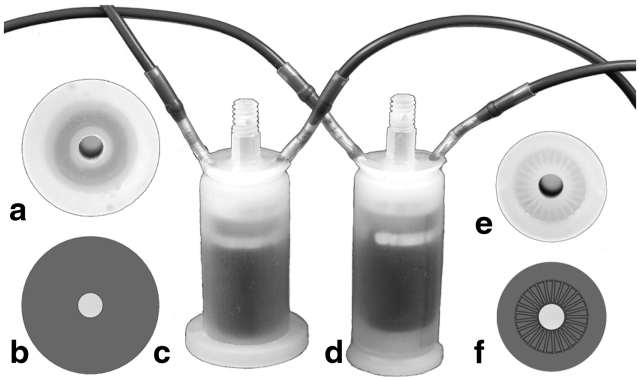

FIG. 3. Completed suckers in the pulling configuration with Dragon Skin 10 cores and skins, VHB 4905 and carbon grease rolled DEAs, rigid attachment points, and electrode leads. A flat-bottom sucker for pressure testing is shown in **(c)**, and a sucker with a bioinspired cup for pull-off testing **(d)**. A photograph of the bottom surface of the flat-bottomed sucker is shown in **(a)**, and a CAD image of it is shown in **(b)**, for clarity. The same is done for the bioinspired sucker with a photograph in **(e)** and a CAD image in **(f)**. CAD, computer-aided design.

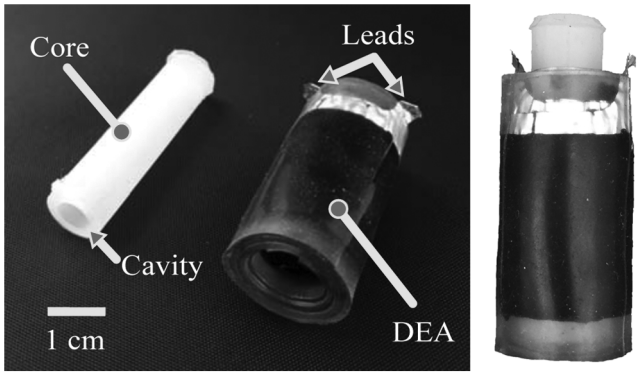

FIG. 4. Sucker core (*left*), DEA removed from core (*center*), and DEA wrapped around the sucker core (*right*).

(in suckers in the pull configuration, only), and an elastomer outer skin. When the sucker is actuated while not sealed to a substrate, the DEA axially extends the inner core, resulting in a net increase of the volume of the cavity within the core similar to pulling the plunger out of a syringe. When the cavity is filled with an incompressible fluid, such as water, and sealed to a substrate, a stress is generated by the DEA in the walls of the cylinder. This stress in the cylinder wall induces a pressure reduction within the cavity without significant volume change or fluid flow. Details on the fabrication and design of each of the four main components of the sucker are listed below.

Sucker inner core

The sucker inner core (Fig. 4) was molded using Dragon Skin 10 silicone elastomer (Smooth-On, Inc.) in a 3D-printed mold (3D Systems ProJet MJP 2500) (Fig. 5). A vacuum chamber was used to degas the elastomer before and after pouring to ensure a proper mold. The core is 10 mm in diameter, 39 mm in height, and has a covered top, a hollow bottom, and a 2 mm wall thickness.

Rolled DEA

Because one of the goals of this study is to leave the top of the actuator free for use with a tension stalk, we chose to use rolled DEAs to create tension within the walls of a cylindrical sucker. Rolled DEAs have been used previously as spring-roll actuators.[28] They are named for the compression spring

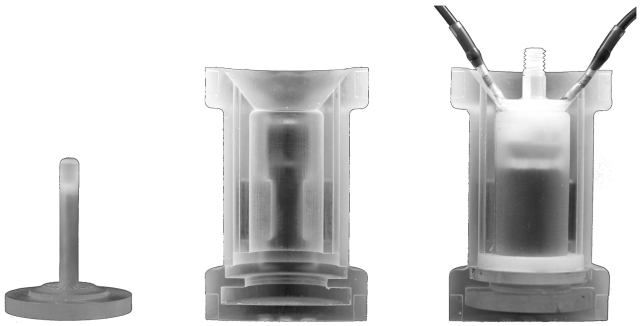

FIG. 5. Sucker core mold insert for bioinspired cup (*left*) and two-part sucker skin mold for flat bottom sucker shown empty (*center*) and with completed sucker (*right*).

that is central to their design. Fabricating these actuators requires biaxially prestraining an elastomer film, applying flexible electrodes (generally carbon grease) to them, and rolling the film around a compressed spring. The spring is released after the film is rolled around it, thereby using stored elastic energy to maintain the prestrain of the elastomer film. To ensure that prestrain is maintained, the elastomer film is fastened to the ends of the spring core by wrapping it around end caps or securing it with pins. While this technique has proven to be effective in creating actuators with large deformations and push-actuation forces,[28] working with prestrained elastomer films requires some form of stiff or rigid support structure to maintain that prestrain. It is also difficult to secure the film to the core without covering the ends of the actuator. For these reasons, we chose to use rolled DEA layers with no prestrain. While DEAs typically exhibit their best performance when they are biaxially prestrained,[29] we show in the Results section that an unprestrained actuator can achieve pressure differentials similar to those of prestrained actuators.

A 3M VHB (very high bond) tape has often been used as the dielectric layer for DEAs in previous studies.[27–30] Various models of the tape are offered that differ in thickness, elasticity, and dielectric constant, among other characteristics. We chose VHB 4905, in particular, for its combination of the above properties.

Fabrication of the rolled DEA was completed as follows:

(1) A VHB 4905 (3M) tape base layer was cut to the size of, and pushed onto, a laser-cut (ULS PLS6MW, 50W CO_2 laser) template.
(2) Two small holes were laser cut into the tape base layer for later electrode degassing.
(3) An aluminum foil electrode lead was pressed onto the top of the first electrode area.
(4) The first carbon grease electrode (MG Chemicals) was brushed over a stencil and any excess carbon grease was removed.
(5) A second layer of unprestrained VHB 4905 tape was applied over the first electrode, leaving 5 mm of tape to tape contact around the first carbon grease electrode.
(6) A second aluminum foil lead was applied to the second layer of VHB tape.
(7) The second carbon grease electrode was brushed over the second layer of VHB tape using a stencil directly above the first electrode.
(8) The film was placed in the laser cutter and cut to the height of the inner core and the proper width (Fig. 6).
(9) The assembled DEA film was rolled around the core. One full roll is a single VHB tape layer, while the second through fourth rolls comprise the DEA layers (two layers of VHB tape and carbon grease electrodes per DEA layer), and the fifth roll is another single VHB tape layer (simplified view shown in Fig. 10).
(10) After rolling, the core and DEA assembly were brought to vacuum to remove any air bubbles in the DEA layers, and heat shrink crimp connectors were attached to the aluminum foil leads.

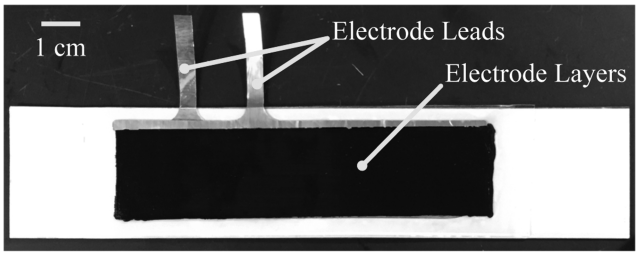

FIG. 6. DEA film on a white backing before rolling onto elastomer core. The film is transparent but covers the white paper backing. The *black rectangle* is composed of two layers of carbon grease electrodes with aluminum foil electrode leads on top.

Three-dimensional-printed attachment point

To attach the sucker to our measuring equipment for pull-off and lifting tests, a 3D-printed insert (Fig. 7) is molded into the top of the inner core and DEA subassembly (for suckers in the pulling configuration only). The geometry of the insert is designed to anchor it within the final sucker. It also includes cutouts for the aluminum foil leads and a threaded shaft for mounting to a load cell. Note that a rigid insert is not required for function of the sucker; it was added in this case for convenience in testing.

Sucker skin

The sucker skin (shown in Fig. 3) encases the sucker core, DEA, and 3D-printed insert in molded Dragon Skin 10. While it is difficult to bond VHB tape and Dragon Skin together, fully encasing the actuator in the outer skin helps to ensure that the DEA stress is transferred to the inner cavity. After curing, the final sucker measures 48 mm tall and 22.5 mm in diameter. It also has either a flat lip (4 mm tall, 32.5 mm diameter) at the bottom or a bioinspired suction cup (5 mm tall, 25 mm outer diameter, 16 mm channel diameter) to ensure a tight seal. All external electrical connections are waterproof, so the sucker can be actuated when fully submerged.

Octopuses increase their attachment force using radial channels in the surface of their suckers (Fig. 8). These

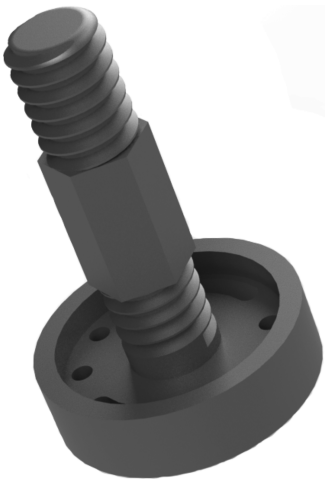

FIG. 7. Render of three-dimensional-printed attachment point for pull-off and lifting tests. This piece is molded to the top of the sucker to attach it to the load cell.

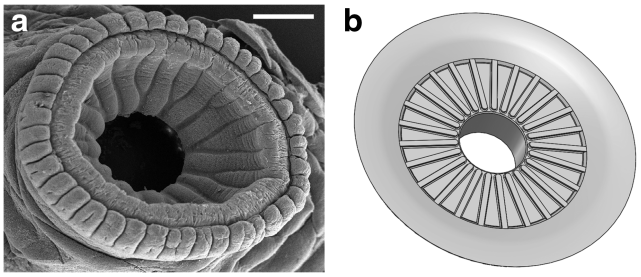

FIG. 8. Scanning electron micrograph of sucker of *Octopus bimaculoides/bimaculatus* **(a)** and bioinspired suction cup design **(b)**. Radial grooves on the octopus sucker spread the pressure differential over a larger area, resulting in larger adhesion forces. Channels are included in the bioinspired cup design to replicate this effect. The scale bar equals 0.5 mm. Left image from work by Kier.[8]

channels spread the pressure differential created by the sucker over a larger area of the substrate, increasing the overall force due to the pressure differential. Adding radial grooves to the bottom surface of our sucker design (shown in Figs. 3e, f, and 8) increases A_{contact} in Equation (17), with a minimal impact on the overall structural integrity of the sucker. This allows for a higher lifting capacity versus a smooth cup of the same size.[12]

Modeling

In this section, we discuss the electrostatic forces created by DEAs, our mechanical modeling of the interactions between DEAs and an elastomer cylindrical pressure vessel, and a model of our design's transient behavior.

DEA mechanics

DEAs can be fabricated in a variety of configurations. This section gives general explanations of planar, cylindrically stacked, and rolled DEA configurations.

Planar DEAs. Planar DEAs (Fig. 9) are essentially parallel plate capacitors. The electric field generated between the plates of a capacitor exerts a force on the plates that attempts to pull them closer to one another. Most capacitors have a fixed geometry, so they do not deform significantly under this force, but DEAs are built using compliant materials, so the electric field generated between the two flexible plates (electrodes) deforms both the electrodes and the dielectric material. When designed properly, this deformation can be used to actuate various devices.[21,31]

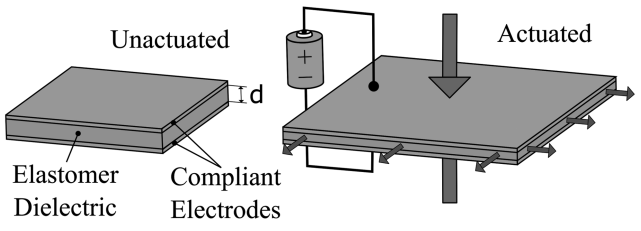

FIG. 9. Ideal planar DEA. When a voltage is applied across the compliant electrodes, the electric field pulls the electrodes together (*large arrows*), resulting in a planar expansion of the elastomer dielectric (*small arrows*).

The normal stress induced in the dielectric material by the generated electric field is the electrostatic pressure[32]

$$p = \varepsilon_0 \varepsilon_r \left(\frac{V}{d}\right)^2, \tag{1}$$

where ε_0 is the permittivity of free space, ε_r is the relative permittivity of the dielectric, V is the voltage across the electrodes, and d is the distance between the electrodes (Fig. 9).

Cylindrically stacked DEAs. Various methods for improving the actuation performance and deformation of DEAs in desired directions have been attempted, including stacking planar DEAs.[30] Stacking DEAs on top of each other increases the net force and/or displacement of the actuator. For this reason, many practical applications of DEAs thus far have involved stacked or rolled (discussed below) actuators.[21] To implement this property in a cylindrical form factor, cylindrical DEAs of increasing radii can be concentrically stacked.

The geometry of planar DEAs is simple, so the only necessary term for the geometry of the DEA in Equation (1) is d, but moving to more complex DEA configurations, such as a cylindrical DEA, leads to more complex geometric terms. A model of the electrostatic pressures and resulting stresses created within cylindrical DEAs is presented in Carpi and De Rossi[33] and adapted for a stacked cylindrical DEA in the Mechanical Modeling section.

Rolled DEAs. While concentrically stacking cylindrical DEAs is the best cylindrical analogue to stacked planar DEAs, it also poses many fabrication challenges (e.g., fabricating cylindrical thin films of varying radii, avoiding air bubbles between layers, and assembling multiple layers). Rolling a planar DEA into a cylinder with multiple DEA layers, as in Pei *et al.*,[28] reduces the difficulty of fabrication while retaining similar actuation characteristics to a cylindrical DEA.[34] This rolled DEA configuration lacks symmetry, increasing the complexity of the geometry and making it more difficult to model.

Mechanical modeling

Here we present a model for calculating the steady-state pressure differential generated by our sucker. We were inspired by the approach used by Carpi and De Rossi[33] and extended their work to a multilayer stacked cylindrical DEA model. Stress and strain fields are derived from the governing differential equation, and kinetic and kinematic boundary conditions are used to solve for the pressure differential generated by the sucker.

Material modeling. To model the sucker, we adopted cylindrical coordinates r, θ, and z with associated displacements u, v, and w. We assume that the system is axisymmetric and that the tangential displacements are negligible. Displacements in the radial and longitudinal directions are assumed to be functions only of coordinates r and z, respectively. Adding the assumption of linear elasticity, Navier's equations for cylindrical coordinates simplify to the

following governing differential equations for each layer of the sucker (shown in Fig. 10):

$$\frac{d}{dr}\left(\frac{1}{r}\frac{d}{dr}(ru)\right)=0\,, \tag{2a}$$

$$\frac{d^2w}{dz^2}=0\,. \tag{2b}$$

The general solutions for the displacements are then solved and expressed as

$$u=c_1\frac{r}{2}+c_2\frac{1}{r}\,, \tag{3a}$$

$$v=0\,, \tag{3b}$$

$$w=c_3z+c_4\,, \tag{3c}$$

in terms of unknown coefficients c_1 through c_4. Here, $c_4=0$ since the origin is defined coincident with the sealing surface.

Subsequently, stresses and strains in cylindrical coordinates can be expressed in terms of the general solution

$$\sigma_r=(\lambda+\mu)c_1-2\mu\frac{c_2}{r^2}+\lambda c_3\,, \tag{4a}$$

$$\sigma_\theta=(\lambda+\mu)c_1+2\mu\frac{c_2}{r^2}+\lambda c_3\,, \tag{4b}$$

$$\sigma_z=\lambda c_1+(\lambda+\mu)c_3\,, \tag{4c}$$

where λ and μ are the Lamé constants, and

$$\varepsilon_r=\frac{c_1}{2}-\frac{c_2}{r^2}\,, \tag{5a}$$

$$\varepsilon_\theta=\frac{c_1}{2}+\frac{c_2}{r^2}\,, \tag{5b}$$

$$\varepsilon_z=c_3\,. \tag{5c}$$

DEA modeling. To account for electrostatic loads, the tractions p applied by the electrodes surrounding a given layer I, as defined by Carpi and De Rossi,[33] are

$$p_a=\frac{\varepsilon V^2}{2\ln^2\left(\frac{r_b}{r_a}\right)r_a^2r_b(r_b^2-r_a^2)}\beta_i, \tag{6a}$$

$$p_b=\frac{\varepsilon V^2}{2\ln^2\left(\frac{r_b}{r_a}\right)r_ar_b^2(r_b^2-r_a^2)}\beta_i, \tag{6b}$$

where a and b denote the inner and outer surface of layer i, respectively, ε is the absolute permittivity, V is the applied voltage, and β is defined as

$$\begin{aligned}\beta_i=[&r_a^6+r_b^6-r_a^2r_b-r_a^4r_b^2\\&+8\ln\left(\frac{r_b}{r_a}\right)(r_b^2-r_a^2)r_a^2r_b^2\\&+4\ln^2\left(\frac{r_b}{r_a}\right)(r_b^2+r_a^2)r_a^2r_b^2]^{0.5}\end{aligned} \tag{7}$$

The electrodes are assumed to be of negligible thickness and stiffness, and it is assumed that there is no slip between the layers.

Kinetic boundary conditions. Solving for the boundary conditions at the interface between layers requires knowledge of the tractions transmitted in both the radial and longitudinal directions. Radial tractions are caused by the electrostatic pressure induced by the DEA, and longitudinal tractions are a result of the varying material properties between layers.

$$\sigma_{r,i}\,|_{r=r_a}=\sigma_{r,i-1}|_{r=r_a}+p_a\,, \tag{8a}$$

$$\sigma_{r,i}\,|_{r=r_b}=\sigma_{r,i+1}|_{r=r_b}+p_b\,, \tag{8b}$$

$$\sigma_{z,i}\,|_{z=h}=t_{z,i}\,. \tag{8c}$$

Tractions due to the electrostatic forces applied by the DEA are considered jump discontinuities at the interfaces between DEA layers. For passive elastomer layers, these tractions are set to zero.

Tractions along the longitudinal axis are in equilibrium with the pressure of the surrounding fluid, p_∞:

$$\sum_{i=1}^{N}[t_{z,i}\pi(r_b^2-r_a^2)]-p_\infty\pi r_{N+1}^2=0\,, \tag{9}$$

where N denotes the total number of layers and p_∞ is the hydrostatic pressure surrounding the sucker.

Kinematic boundary conditions. Since the sucker's deformation is assumed to be continuous, the kinematic boundary conditions at each interface are assumed equal, with $r_{b,i}$ and $r_{a,i+1}$ denoting the outer and inner radii of their respective layers,

$$u_i|_{r=r_{b,i}}=u_{i+1}|_{r=r_{a,i+1}}\,. \tag{10}$$

Finally, the fluid inside the cavity is assumed to be incompressible. As a result, the relationship between the longitudinal and radial strain at the cavity wall $r=r_1$ is expressed as follows:

$$\pi r_1^2|_{t=0}\;h_0=\pi r_1^2|_{t=f}\;h_f\,, \tag{11}$$

evaluated at the initial and final configurations; therefore,

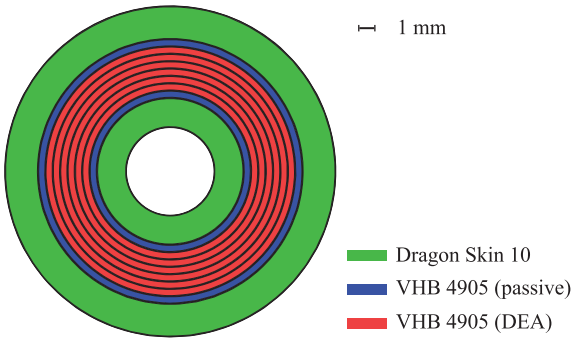

FIG. 10. Simplified schematic of the layers in the artificial sucker design. This configuration is used for pressure response modeling, but the physical sucker has a DEA spiral as a result of the rolled DEA configuration, as opposed to the cylindrically stacked configuration shown here. Color images are available online.

$$\varepsilon_z = (\varepsilon_r|_{r=r_1} + 1)^{-2} - 1. \tag{12}$$

To predict the pressure differential generated by the sucker, we start by inserting a given input voltage into the DEA dynamics equation, Equation (6), to get the induced tractions. Then, by imposing the kinetic and kinematic boundary conditions on the stress and strain fields, Equations (4) and (5), we solve for the unknown coefficients c_1, c_2, and c_3 in each layer using a nonlinear numerical solver.

Cylindrical pressure vessel modeling. Once the stresses within the cavity wall are known, calculating the pressure inside the sucker's cavity becomes a simple force balance that depends solely on the geometry of the sucker. Here we show these force balances for a decapod-like geometry (a cylindrical pressure vessel).

The wall stresses in a cylindrical pressure vessel (Fig. 11) vary with a change in direction tangent to the surface of the pressure vessel. If a plane bisects the cylinder normal to the axis of the cylinder, the stresses in the wall normal to that plane are referred to as longitudinal stresses (σ_z). When the bisecting plane is coincident with the axis of the cylinder, the stress normal to the bisecting plane is referred to as tangential stress (σ_θ). The effect of longitudinal stress on the pressure differential ΔP is defined by balancing the forces from stress in the normal cut with

$$\pi((r+t)^2 - r^2)\sigma_z = \pi r^2 \Delta P. \tag{13}$$

Rearranging for ΔP yields the following:

$$\Delta P = P_1 - P_2 = \sigma_z(2rt + t^2)/r^2. \tag{14}$$

The force balance for tangential stress is defined as

$$2ht\sigma_\theta = 2rh\Delta P. \tag{15}$$

Rearranging for ΔP yields a second relationship for the pressure differential in a cylindrical pressure vessel:

$$\Delta P = t\sigma_\theta / r. \tag{16}$$

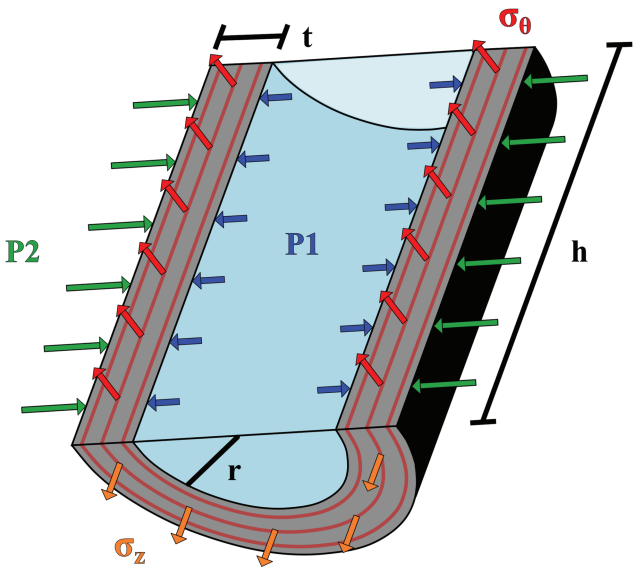

FIG. 11. Cylindrical pressure vessel bisected by two normal planes coincident with and perpendicular to the axis of the cylinder, respectively. *Red lines* represent DEA layers that compress radially when actuated to create the longitudinal stress σ_z (*orange arrows*) parallel to the cylinder's axis and the tangential stress σ_θ (*red arrows*) perpendicular to the bisecting plane coincident with the cylinder's axis. A force balance can be applied to each of the bisecting planes to calculate the pressure differential between P_1 (*blue arrows*) and P_2 (*green arrows*) in terms of σ_z and σ_θ. Color images are available online.

The suction force (F_{suction}) is equal to the pressure differential [Equations (14) or (16)] multiplied by the area (A_{contact}) of the sucker cavity on the surface:

$$F_{\text{suction}} = A_{\text{contact}}\Delta P = \pi r^2 \Delta P. \tag{17}$$

Transient behavior

Assuming the viscoelastic response of the sucker and the DEA's change in capacitance are small for small deformations, the transient response of the sucker should be a function of the electrostatic pressure. The DEA's transient behavior, and therefore the behavior of the electrostatic pressure created, can be roughly described as that of a charging capacitor: $V = R\dot{Q} + Q/C$, where R is electrical resistance, C is capacitance, and Q is charge. Solving this equation for its transient behavior yields $Q/CV = 1 - e^{-t/\tau}$, where the time constant τ is sample dependent. This form leads to the sucker's transient pressure equation:

$$P_{\text{transient}}(t, V) = (1 - e^{-t/c_2})P_{ss}(V), \tag{18}$$

where c_2 can be fit to the data to account for unmodeled material interactions within the sucker and $P_{ss}(V)$ is the steady-state pressure at a constant voltage V.

Experimental Procedure

In this section, we describe the equipment and procedure used for pressure generation, pull-off, and lifting experiments.

Equipment

High-voltage test enclosure. Our group designed a high-voltage enclosure to test DEAs (Fig. 12). It utilizes an UltraVolt 10A24-P15-I5 high-voltage module to generate up to 10.75 kV. Voltage and current are controlled and measured through a National Instruments NI PCI-6221 data acquisition card in conjunction with a LabVIEW VI. Other test equipment, such as the load cell and linear actuator used for pull-off and lifting tests, are mounted and controlled within the enclosure.

Sucker test tank. Pressure changes within the sucker were recorded in a small test tank (Fig. 13) using either a Freescale sensor MPXV7007DP or MPXV7025DP differential pressure sensor. The ports of the sensor were connected to ports on the bottom of the tank such that one port was centered under the sucker cavity and the other opened to the bottom of the tank outside the cavity. All tests were performed with the sucker fully submerged in water.

Pressure generation test

Pressure generation tests consisted of a voltage sweep using square waves increasing from 2.75 to 10.75 kV in 1 kV increments with a period of 20 s and a duty cycle of 50% to characterize the sucker's voltage response and transient behavior. For each actuation cycle, the last 1.0 s of actuation was averaged and recorded as the maximum achieved pressure at that voltage. An acrylic alignment plate was used to center the sucker over the pressure port and ensure a seal between the sucker and the tank bottom. This test was conducted on suckers in both the fully soft and pulling configurations.

Pull-off test

Pull-off tests have been used as a metric for the strength of both biological and artificial cephalopod suction cups.[9,12,24,25] For this test, the sucker was aligned in the test tank as described in the Sucker Test Tank section. For each pull, a linear stage (Zaber T-LA60A linear actuator and Zaber TSB60-I translation stage) pushed the sucker to the bottom of the tank with a force of 7 N, the DEA was actuated at voltages varying from 2.75 to 10.75 kV (except for the unactuated, 0 kV case), and the linear stage pulled the sucker at a constant velocity until the sucker detached from the bottom of the tank while pressure and force data were recorded. Force data were collected using a PCB Piezotronics 1102-05A load cell. Pull-off tests were conducted only on the sucker with a bioinspired cup in the pulling configuration.

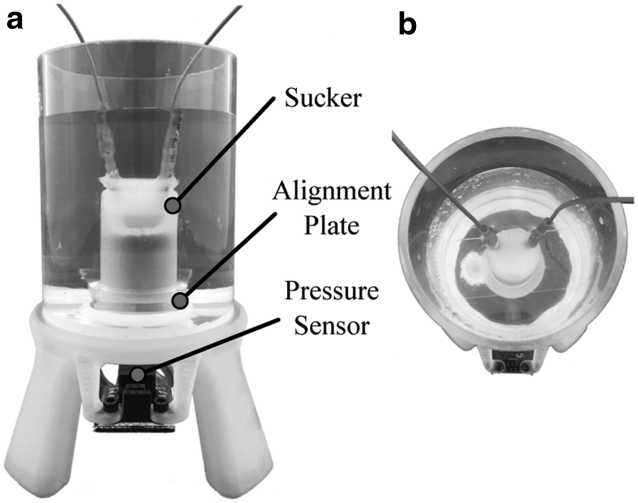

FIG. 13. Pressure test tank front **(a)** and top **(b)** views. The rim of the sucker is centered above a pressure port and pushed against the bottom of the tank by an acrylic plate.

Lifting test

Objects of a range of masses were lifted with the artificial sucker to validate the pull-off testing (Fig. 14). For these tests, an object was placed in a small aquarium filled with

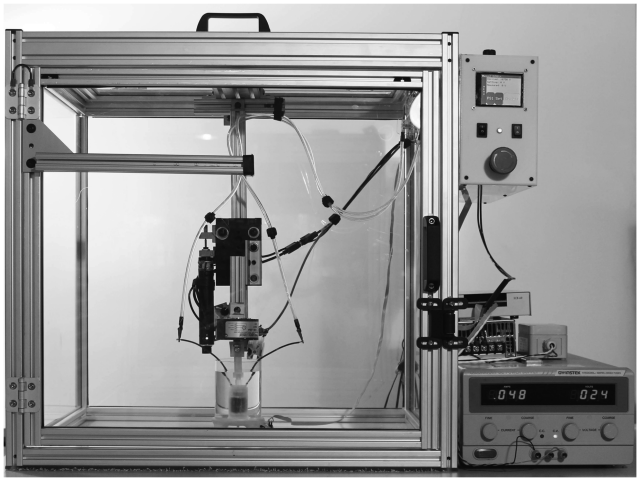

FIG. 12. The high-voltage test enclosure can generate and safely contain voltages up to 10.75 kV. All tests were conducted within this enclosure and shown here configured for pull-off testing.

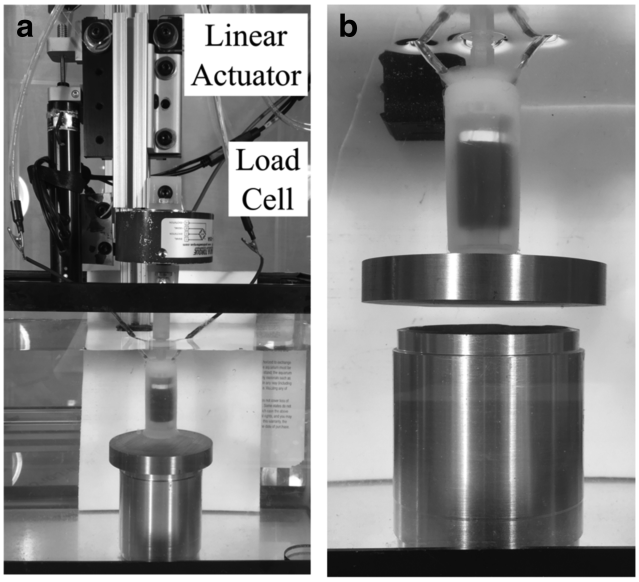

FIG. 14. Lifting test setup **(a)** and sucker lifting a 441 g steel disk **(b)**. The cylinder sitting in the aquarium was used to support the object being lifted to prevent Stefan adhesion forces from holding the object on the glass aquarium bottom.

water, the linear stage was used to push the sucker onto the object with a force of 7 N, the DEA was activated at 10.75 kV, and the linear stage lifted the sucker and attached object while the load cell recorded forces on the sucker. Lifting tests were conducted only on the sucker with a bioinspired cup in the pulling configuration.

Results

Here we report the data from our pressure-generation experiment as a function of voltage (Steady-State Pressure Response section) and time (Transient Response section) and our pull-off test results validated by lifting tests (Pull-Off and Lifting Tests section).

Steady-state pressure response

Pressure data for each sucker are shown as a function of applied voltage and compared to our mechanical model in Figure 15. The fully soft sucker generated a maximum pressure differential of 3.63 ± 0.07 kPa (±SD) at 10.76 kV in the 1 s measured. The sucker in the pulling configuration generated a maximum pressure differential of 2.74 ± 0.10 kPa (±SD) at 10.76 kV. These data are consistent with the model presented in the Mechanical Modeling section, within an average error of 15.5%.

Since data were only taken for voltages up to 10.75kV to avoid dielectric breakdown of the suckers, a higher pressure differential is theoretically possible. The triangles in Figure 15 indicate where dielectric breakdown should occur (12.4 kV, calculated using the 25 V/μm dielectric strength of VHB 4905 and a 0.5 mm thickness, according to the 3M datasheet). According to this analysis, the theoretical maximum pressure differential obtainable by this design is 4.90 kPa for the fully soft sucker and 3.81 kPa for the sucker in the pulling configuration.

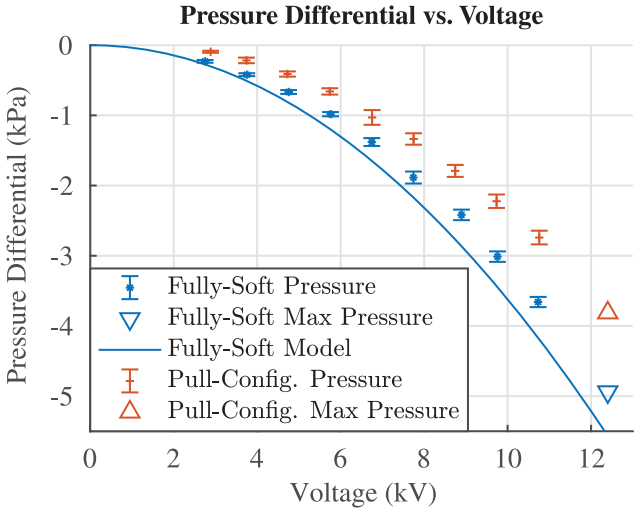

FIG. 15. Maximum pressure differential as a function of voltage for the suckers in the fully soft and pulling configurations. While the voltage source used is not capable of causing dielectric breakdown of the actuator, it is possible to predict that the actuator will break down at 12.4 kV. When actuated at 12.4 kV, the suckers in the fully soft and pulling configurations should be capable of generating 4.90 kPa and 3.81 kPa pressure differentials, respectively. The error bars shown are for the standard deviation between data sets. Color images are available online.

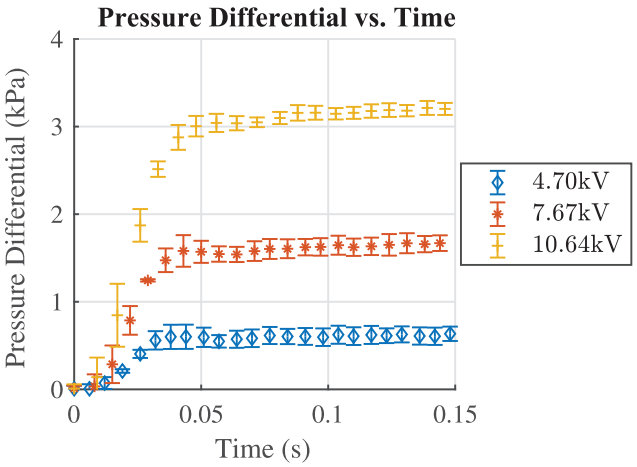

FIG. 16. Experimental pressure differential as a function of time for all actuation voltages. Every eighth data point is plotted for clarity. The error bars shown are for the standard deviation between data sets. Color images are available online.

Transient response

The transient pressure response of the fully soft artificial sucker is shown in Figure 16. Normalizing these data by the maximum pressure differential at each of several voltages collapses these values, Figure 17. The Transient Behavior section presents the expected behavior of $P_{\text{transient}}$ in Equation (18), and fitting c_2 yields

$$P_{\text{transient}}(t, V) = (1 - e^{-t/0.0125s}) P_{ss}(V), \tag{19}$$

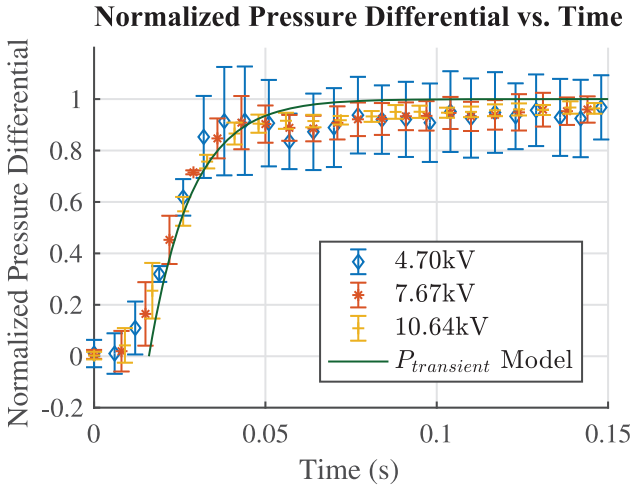

FIG. 17. Pressure readings normalized by the maximum pressure produced at several actuation voltages (intermediate voltages omitted for clarity). The slow response during the first 16 ms of actuation corresponds to the activation time of the power supply. Every eighth data point is plotted for clarity. The error bars shown are for the standard deviation between data sets. Color images are available online.

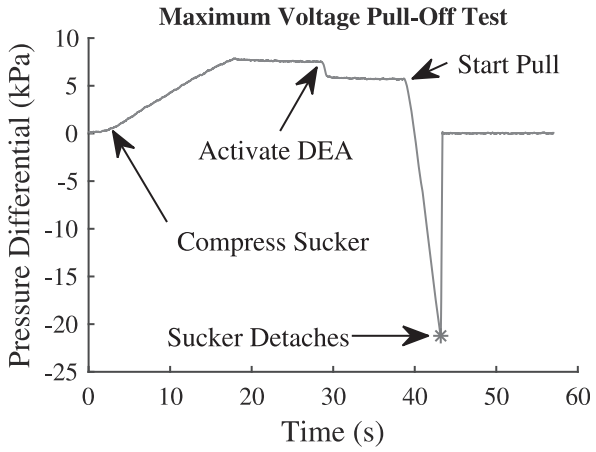

FIG. 18. Experimental sucker pressure differential as a function of time when actuated at 10.74 kV. Key points in testing are labeled. The point when the sucker detached from the substrate, marked by a *star*, is saved for each actuation voltage and reported in Figure 19.

where c_2 was fit using the least squares method. Data before $t = 16$ ms were ignored during fitting to account for the activation time of the power supply.

Pull-off and lifting tests

A sample pull-off test is shown in Figure 18, and a summary of all pull-off tests as a function of voltage is shown in Figure 19. Both force and pressure data were filtered using a running average filter with a span of eight data points. The sucker was observed to pull with a maximum force of 8.34 ± 0.10 N (±SD) and generate a pressure differential of 21.34 ± 0.44 kPa (±SD) at pull-off when the DEA was actuated at 10.75 kV. The data indicate a nonlinear relation to voltage, and the DEA actuation has a multiplicative effect on pull-off force and maximum pressure differential (Fig. 20) (discussed further in the Experimental Procedure section). The pull-off tests were validated by lifting an 800 g mass, which exerted 5.33 N on the sucker (due to buoyant forces).

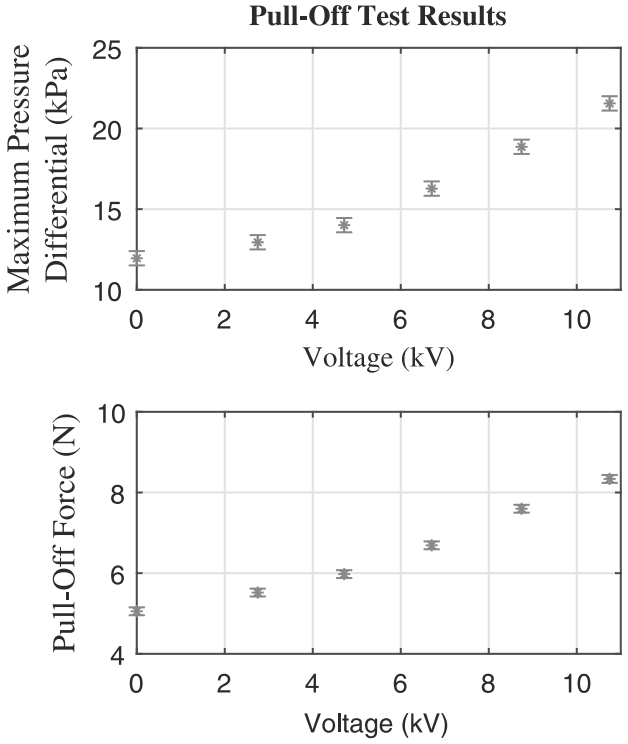

FIG. 19. Experimental maximum sucker pressure differential and pull-off force as a function of DEA voltage during pull-off testing. Each data point, represented by a star, is determined as shown in Figure 18. The error bars shown are for the standard deviation between data sets.

Discussion

As shown in Figure 17, the sucker reaches 90% of its steady-state value in ~50 ms, regardless of the input voltage. This supports the claim that the dominant transient response of the sucker (19) is equivalent to that of a plate capacitor.

While the reported data are promising, the observed losses in generated pressure differential from the model to the fully soft sucker's experimental results are likely due to the geometry and composition of the artificial sucker. One such factor may be slippage between the DEA layers. The DEA successfully creates a stress in the wall of the cylinder, but the carbon grease used as the DEA's compliant electrode prevents the VHB tape layers from bonding together, potentially resulting in slippage between the layers and a reduced net stress in the cavity. Another factor is that the rolled design that was fabricated may not perform as well as the cylindrically stacked design that was modeled. Other losses could be caused by unintended deformation of the skin and core, both as a result of actuation and/or the environment.

Additional pressure generation losses in the sucker in the pulling configuration are likely due to the rigid insert's resistance to radial deformation. Since the actuation of the DEA

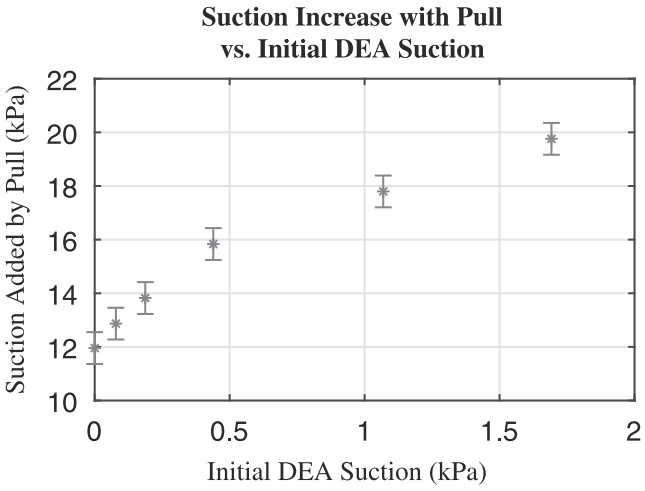

FIG. 20. Increase in suction pressure during pull-off test ($P_{max} - P_{DEA}$) versus initial DEA suction (P_{DEA}). Activating the DEA has a greater impact on overall suction than simply adding its own generated pressure during pull-off testing. $P_{\_max}$ is represented by each star in Figure 19, while $P_{\_DEA}$ is the difference between the measured pressure differentials before and after DEA activation, shown in Figure 18. The error bars shown are for the standard deviation between data sets.

is mainly due to stress in the radial direction, inhibiting deformation in the radial direction inhibits the DEA's ability to actuate, at least near the top of the sucker.

The rise time of the pressure response is slightly shorter for lower voltage inputs (Fig. 16). The differences in response times are possibly due to the viscoelastic properties of the elastomers used. Viscoelastic materials are stiffer at higher strain rates, and since higher voltages cause the elastomers to deform faster, the higher strain rates at these higher voltages may stiffen the elastomers in the artificial sucker, thereby increasing the rise time.

Pull-off testing indicates that our initial hypothesis that a small pressure differential created by a DEA would create a sufficient initial force to allow for useful actuation forces when pulling on the sucker was confirmed. The trend shown in Figure 20 suggests that not only does the DEA enable this behavior but it also has a multiplicative effect on the pull-off force achieved. This could be due to a reduction in the DEA dielectric layer thickness while the sucker is stretched during lifting. According to Equation (1), a reduction in DEA layer thickness exponentially increases the electrostatic pressure generated by the DEA. As the DEA will continue to deform with increasing electrostatic pressure, the DEA stress and the stress due to the external lifting force will continue to augment the DEA's effect until either an equilibrium point is reached or the sucker's seal fails. Existing DEA-based suction designs rely purely on the DEA to create a pressure differential, but this design's geometry utilizes the extra deformation from external forces to magnify the DEA's effect and generate much higher suction forces.

Not only does this effect increase the lifting capacity of this end effector but it makes releasing an object easier as well. Lifted objects can be dropped on command simply by deactivating the DEA since no fluid was removed from the cavity to create suction. Once the DEA is deactivated, the compounding effect caused by the interaction between the DEA and external pulling forces vanishes, returning the sucker to an unactuated state and greatly reducing its effectiveness.

As stated above, the DEA significantly enhances pull-off forces once it is activated. Due to the sucker's cup geometry, an external force on the sucker is still required to initiate a seal with the substrate. Typically, inactive suction cups require a similar force to push fluid out of the sucker's cavity, creating the entirety of the negative pressure differential on release, but this should not be confused with the mechanism in effect in our sucker. As shown in Figures 19 and 20, while there was likely some small fluid flux out of the sucker, as evidenced by the nonzero pressure differential and suction force at 0 kV, the DEA nearly doubles the maximum pull-off force and pressure differential. The DEA also does not require fluid flux out of the sucker to generate a pressure differential, as shown in Figure 15 where there was no push force applied to the top of the sucker.

The maximum attachment force of an underwater sucker increases with depth, giving artificial suckers tremendous potential for deep water applications. This can be explained as follows. For a given size sucker, as shown in Equation (17), the attachment force is determined by the pressure differential between the water inside the cavity and the pressure outside the sucker. The pressure outside the sucker increases by ~ 100 kPa with each 10 m depth increase. The minimum pressure inside the sucker is limited by the water's tensile strength. A sucker can reduce the pressure until tension in the water reaches a critical value and the water cavitates.[25,35] This minimum pressure is known as the cavitation threshold. Because the cavitation threshold is relatively independent of depth, and ambient pressure increases with depth, the maximum possible pressure differential, and thus the force of attachment, increases with depth.[36] Thus, an artificial sucker capable of high actuation stresses could potentially generate unusually large attachment forces in deep water.

Conclusions

Unlike many other DEA-driven soft robotic devices, our artificial sucker is soft and waterproof. Other devices rely on rigid frames to maintain prestrain in the DEA layers, but our design could be implemented on a fully soft system. This unprestrained, entirely soft, rolled DEA configuration generates pressure differentials that rival those presented in the existing literature on DEA-generated suction, suggesting that DEAs can be used for actuation without the difficulties that accompany prestrained DEA fabrication. Pull-off and object lifting tests have shown that this sucker is capable of being used on a compact AUV for low-power reversible attachment.

While our goal was to show that DEAs can be used in an artificial sucker aboard a compact AUV, this design has many applications outside of the underwater robotic realm. Miniaturized artificial suckers of this kind have the potential to provide a compliant and gentle method of attachment to biological tissue during surgical procedures. This gentle attachment could also be used when collecting marine animal and plant specimens without damage.

Future work will involve modeling the dynamic behavior of the artificial sucker, including viscoelastic effects, a scalability study, a geometric study, and implementation on an AUV. The scalability study should include an assessment of the scalability of DEAs as it pertains to the generation of a pressure differential as well as an evaluation of cavity size on measured pressures. The geometric study should investigate the optimal geometry of the artificial sucker to minimize losses due to undesired deformation.

Acknowledgments

This work was partially supported by the Office of Naval Research and the National Science Foundation. The first author was funded by the University of Florida Graduate School Fellowship Program, the Robert C. Pittman Fellowship Endowment, and the Department of Defense (DoD) through the National Defense Science & Engineering Graduate Fellowship (NDSEG) Program. The second author was funded by the University of Florida Graduate School Fellowship Program. The Florida affiliated authors would like to thank Mike Krieg for helpful discussions about various aspects of fabrication and modeling reported in this manuscript, Ajay Dass for his help with fabricating samples, and Robyn Natherson for her assistance with testing.

Author Disclosure Statement

No competing financial interests exist.

References

1. Levy G, Flash T, Hochner B. Arm coordination in octopus crawling involves unique motor control strategies. Curr Biol 2015;25:1195–1200.
2. Richter JN, Hochner B, Kuba MJ. Octopus arm movements under constrained conditions: adaptation, modification and plasticity of motor primitives. J Exp Biol 2015;218:1069–1076.
3. Sumbre G, Fiorito G, Flash T, *et al.* Motor control of flexible octopus arms. Nature 2005;433:595–596.
4. Messenger J. The visual attack of the cuttlefish, Sepia officinalis. Anim Behav 1968;16:342–357.
5. Kier WM, VanLeeuwen JL. A kinematic analysis of tentacle extension in the squid Loligo pealei. J Exp Biol 1997; 200:41–53.
6. Mann J, Patterson EM. Tool use by aquatic animals. Philos Trans R Soc Lond B Biol Sci 2013;368:11.
7. Kier WM, Smith AM. The morphology and mechanics of octopus suckers. Biol Bull 1990;178:126–136.
8. Kier WM, Smith AM. The structure and adhesive mechanism of octopus suckers. Integr Comp Biol 2002;42:1146–1153.
9. Bandyopadhyay PR, Hrubes JD, Leinhos HA. Biorobotic adhesion in water using suction cups. Bioinspir Biomim 2008;3:11.
10. Hu BS, Wang LW, Fu ZA, *et al.* Bio-inspired miniature suction cups actuated by shape memory alloy. Int J Adv Robot Syst 2009;6:151–160.
11. Tramacere F, Beccai L, Mattioli F, *et al.* Artificial adhesion mechanisms inspired by octopus suckers. In: Proceedings of the IEEE International Conference on Robotics and Automation (ICRA), Saint Paul, MN. 2012, pp. 3846–3851.
12. Tramacere F, Follador M, Pugno NM, *et al.* Octopus-like suction cups: from natural to artificial solutions. Bioinspir Biomim 2015;10:8.
13. Kuwajima Y, Shigemune H, Cacucciolo V, *et al.* Active suction cup actuated by ElectroHydroDynamics phenomenon. In: 2017 IEEE/RSJ International Conference on Intelligent Robots and Systems (IROS). Vancouver, Canada: 2017, pp. 470–475.
14. Krieg M, Klein P, Hodgkinson R, *et al.* A hybrid class underwater vehicle: bioinspired propulsion, embedded system, and acoustic communication and localization system. Mar Technol Soc J 2011;45:153–164.
15. Song ZY, Mazzola C, Schwartz E, *et al.* A compact autonomous underwater vehicle with cephalopod-inspired propulsion. Mar Technol Soc J 2016;50:88–101.
16. Laschi C, Mazzolai B, Cianchetti M. Soft robotics: technologies and systems pushing the boundaries of robot abilities. Sci Robot 2016. DOI: 10.1126/scirobotics.aah3690.
17. Renda F, Giorelli M, Calisti M, *et al.* Dynamic Model of a multibending soft robot arm driven by cables. IEEE Trans Robot 2014;30:1109–1122.
18. Umedachi T, Vikas V, Trimmer BA. Softworms: the design and control of non-pneumatic, 3D-printed, deformable robots. Bioinspir Biomim 2016;11:16.
19. Cianchetti M, Calisti M, Margheri L, *et al.* Bioinspired locomotion and grasping in water: the soft eight-arm OCTOPUS robot. Bioinspir Biomim 2015;10:19.
20. Madsen FB, Daugaard AE, Hvilsted S, *et al.* The current state of silicone-based dielectric elastomer transducers. Macromol Rapid Commun 2016;37:378–413.
21. Anderson IA, Gisby TA, McKay TG, *et al.* Multi-functional dielectric elastomer artificial muscles for soft and smart machines. J Appl Phys 2012;112:20.
22. Grasso FW, Setlur P. Inspiration, simulation and design for smart robot manipulators from the sucker actuation mechanism of cephalopods. Bioinspir Biomim 2007;2:S170–S181.
23. Tramacere F, Pugno NM, Kuba MJ, *et al.* Unveiling the morphology of the acetabulum in octopus suckers and its role in attachment. Interface Focus 2015;5:5.
24. Hou JP, Wright E, Bonser RHC, *et al.* Development of biomimetic squid-inspired suckers. J Bionic Eng 2012;9: 484–493.
25. Smith AM. Cephalopod sucker design and the physical limits to negative pressure. J Exp Biol 1996;199:949–958.
26. Williams LW. The Anatomy of the Common Squid. Leiden, Holland: Library and printing office late E.J. Brill. 1910, pp. 1–92.
27. Follador M, Tramacere F, Mazzolai B. Dielectric elastomer actuators for octopus inspired suction cups. Bioinspir Biomim 2014;9:10.
28. Pei Q, Rosenthal M, Stanford S, *et al.* Multiple-degrees-of-freedom electroelastomer roll actuators. Smart Mater Struct 2004;13:N86–N92.
29. Pelrine R, Kornbluh R, Pei QB, *et al.* High-speed electrically actuated elastomers with strain greater than 100%. Science 2000;287:836–839.
30. Kovacs G, During L, Michel S, *et al.* Stacked dielectric elastomer actuator for tensile force transmission. Sens Actuators A Phys 2009;155:299–307.
31. Rus D, Tolley MT. Design, fabrication and control of soft robots. Nature 2015;521:467–475.
32. Pelrine RE, Kornbluh RD, Joseph JP. Electrostriction of polymer dielectrics with compliant electrodes as a means of actuation. Sens Actuators A Phys 1998;64:77–85.
33. Carpi F, De Rossi D. Dielectric elastomer cylindrical actuators: electromechanical modelling and experimental evaluation. Mater Sci Eng C Biomim Supramol Syst 2004; 24:555–562.
34. Wang HM, Li LY, Zhu YL, *et al.* Analysis and application of a rolled dielectric elastomer actuator with two degrees of freedom. Smart Mater Struct 2016;25:11.
35. Smith AM. Negative-pressure generated by octopus suckers—a study of the tensile-strength of water in nature. J Exp Biol 1991;157:257–271.
36. Smith AM, Kier WM, Johnsen S. The effect of depth on the attachment force of limpets. Biol Bull 1993;184:338–341.

Address correspondence to:
Kamran Mohseni
Department of Mechanical and Aerospace Engineering
University of Florida
PO Box 116250
Gainesville, FL 32611

E-mail: mohseni@ufl.edu